Unraveling Oxygen Reduction Reaction Mechanisms on Carbon-Supported Fe-Phthalocyanine and Co-Phthalocyanine Catalysts in Alkaline Solutions

Rongrong Chen,*,† Haixia Li,† Deryn Chu,‡ and Guofeng Wang*,†,§

Richard G. Lugar Center for Renewable Energy, Indiana University Purdue University−Indianapolis, Indianapolis, Indiana 46202, U.S. Army Research Laboratory, Adelphi, Maryland 20783, and Department of Mechanical Engineering, Indiana University Purdue University−Indianapolis, Indianapolis, Indiana 46202

Received: July 7, 2009; Revised Manuscript Received: October 13, 2009

In this work, we combine electrochemical measurements, such as the rotating disk electrode (RDE) and the rotating ring-disk electrode (RRDE) techniques, and density functional theory (DFT) calculations to elucidate the mechanisms of the oxygen reduction reaction (ORR) on carbon-supported Fe-phthalocyanine (FePc/C) and Co-phthalocyanine (CoPc/C) catalysts in 0.1 M NaOH solutions. The onset potential for ORR on FePc/C catalyst is found to be around 0.05 V vs. Hg/HgO in 0.1 M NaOH solutions, which is 100 mV more positive than that on CoPc/C. RDE and RRDE measurements show that the ORR mechanism is via a $4e^-$ pathway on the FePc/C while it is through a $2e^-$ pathway on the CoPc/C catalyst. The catalyst stability tests reveal that FePc is much less stable than CoPc under fuel cell cathode working conditions. Moreover, DFT calculations were performed to study the adsorption of O_2, H_2O, OH, HOOH, and H_2OO molecules on FePc and CoPc molecule catalysts. We conclude the following from our theoretical and experimental results for the ORR on FePc/C and CoPc/C catalysts: (1) the lower the O_2 adsorption energy, the higher the kinetics of the ORR will be; (2) the ORR pathways, $2e^-$ or $4e^-$, are mainly determined by the H_2O_2 adsorption configurations; and (3) OH adsorption on the catalysts is considered to be an important factor to affect the catalyst stability.

I. Introduction

Recently there has been a growing worldwide interest in developing solid alkaline fuel cells (SAFCs), which have various applications as low-cost yet high-performance power sources.[1–10] Compared to liquid alkaline fuel cells (AFCs) and proton exchange membrane fuel cells (PEMFCs), SAFCs possess several important merits, including (1) facile kinetics at the cathode and the anode, (2) minimal methanol/ethanol crossover effect, (3) simplified water management, (4) no precipitated carbonate, (5) no electrolyte weeping, and (6) a wide choice of materials for current supports, bipolar plates, and fuel cells. To advance the technology of SAFCs, we have been developing novel alkaline anion exchange membranes[11,12] and investigating various transition metals[13,14] as well as transition metals of N_4-macrocycles (M-N_4-macrocycles) as electrocatalysts to replace Pt for the oxygen reduction reaction (ORR) in alkaline media.

M-N_4-macrocycles, such as porphyrins and phthalocyanines, have been considered as promising catalysts for the ORR[15–28] in alkaline and acid media for several decades. It has been established that (1) the type of central metal atom determinatively influences their catalytic activity, (2) their polymeric or heat-treated M-N_4 forms could lead to better chemical and thermal stabilities, higher electronic conductivities, and higher O_2 activities[23–25] than their monomeric species, and (3) the pH values of electrolytes affect the activities and stabilities of the catalysts.[16] Despite much effort in developing M-N_4-macrocycles as fuel cell electrocatalysts, so far, no macrocycle molecule catalysts have demonstrated acceptable ORR catalytic activity and stability as compared to Pt-based catalysts. At the moment, lacking a fundamental understanding of the catalytic activity and stability of these catalyst molecules hinders further development for their practical applications. In this paper, we combine electrochemical measurements, such as the rotating disk electrode (RDE) and the rotating ring-disk electrode (RRDE) techniques, and density functional theory (DFT) calculations to elucidate the mechanisms of the ORR on carbon-supported Fe-phthalocyanine (FePc/C) and Co-phthalocyanine (CoPc/C) in alkaline media. The synergic combination of theory and experiments enables us to better interpret the ORR overpotential, the reaction pathways, and the stability of these catalysts.

The electrochemical reduction of O_2 is a multielectron reaction that has two main possible pathways: one involving the transfer of two electrons to produce H_2O_2, and the other, a direct four-electron pathway to produce water. In alkaline media, the $2e^-$ pathway can be written[25] as:

$$O_2 + H_2O + 2e^- \rightarrow HO_2^- + OH^- \qquad E_0 = -0.230 \text{ V vs. Hg/HgO (0.1 M NaOH)} \quad (1)$$

The direct $4e^-$ pathway can be written as:

$$O_2 + 2H_2O + 4e^- \rightarrow 4OH^- \qquad E_0 = 0.236 \text{ V vs. Hg/HgO (0.1 M NaOH)} \quad (2)$$

To obtain maximum energy capacity, it is highly desirable to reduce O_2 via the $4e^-$ pathway. Precious Pt and its alloys are known to promote the $4e^-$ ORR pathway. For Pt and other metallic catalysts, DFT calculations have been successfully

* To whom correspondence should be addressed. E-mail: rochen@iupui.edu (R.C.) or wang83@iupui.edu (G.W.).
† Richard G. Lugar Center for Renewable Energy, Indiana University Purdue University Indianapolis.
‡ U.S. Army Research Laboratory.
§ Department of Mechanical Engineering, Indiana University Purdue University Indianapolis.

10.1021/jp906408y CCC: $40.75
Published on Web 11/09/2009

Report Documentation Page

Form Approved
OMB No. 0704-0188

1. REPORT DATE	2. REPORT TYPE	3. DATES COVERED
13 OCT 2009		**00-00-2009 to 00-00-2009**

4. TITLE AND SUBTITLE	5a. CONTRACT NUMBER
Unraveling Oxygen Reduction Reaction Mechanisms on Carbon-Supported Fe-Phthalocyanine and Co-Phthalocyanine Catalysts in Alkaline Solutions	5b. GRANT NUMBER
	5c. PROGRAM ELEMENT NUMBER
6. AUTHOR(S)	5d. PROJECT NUMBER
	5e. TASK NUMBER
	5f. WORK UNIT NUMBER
7. PERFORMING ORGANIZATION NAME(S) AND ADDRESS(ES) **Richard G. Lugar Center for Renewable Energy,Indiana University Purdue University,Indianapolis,IN**	8. PERFORMING ORGANIZATION REPORT NUMBER
9. SPONSORING/MONITORING AGENCY NAME(S) AND ADDRESS(ES)	10. SPONSOR/MONITOR'S ACRONYM(S)
	11. SPONSOR/MONITOR'S REPORT NUMBER(S)

12. DISTRIBUTION/AVAILABILITY STATEMENT
Approved for public release; distribution unlimited

13. SUPPLEMENTARY NOTES

14. ABSTRACT

15. SUBJECT TERMS

16. SECURITY CLASSIFICATION OF:			17. LIMITATION OF ABSTRACT	18. NUMBER OF PAGES	19a. NAME OF RESPONSIBLE PERSON
a. REPORT	b. ABSTRACT	c. THIS PAGE			
unclassified	**unclassified**	**unclassified**	**Public Release**	**9**	

applied to elucidate the origin of the overpotential of the ORR,[29] the mechanism of the ORR in acids,[30] and the alloying effect on the catalytic activity for the ORR.[31] However, a similar study is scarce for other catalyst systems like M-N_4-macrocycles. Recently we reported our work[32] studying the adsorption of oxygen molecules on FePc and CoPc molecules using the DFT method. We found that there are multiple stable adsorption configurations for O_2 adsorbed on FePc and CoPc molecules. Extending our prior work, here we performed detailed DFT calculations for O_2, H_2O, OH, and H_2O_2 molecule adsorption on the surfaces of FePc and CoPc in order to gain insights into the ORR mechanism on those catalyst molecules.

II. Experimental and Theoretical Methods

II.1. Materials. The FePc and CoPc were purchased from Alfa Aesar and used as received. To disperse FePc or CoPc on a high surface area carbon substrate (Vulcan XC-72, CABOT Corp., Boston, MA, USA), 86.340 mg of FePc or CoPc was first weighted, dissolved in concentrated H_2SO_4, and sonicated for 30 min. After complete dissolution of the FePc or CoPc in the H_2SO_4 solution, 0.2 g of Vulcan XC-72 carbon supports was added into the solution which was ultrasonically homogenized to form a suspension of FePc or CoPc dispersed on carbon supports. Then the suspension was poured into cold deionized (DI) water, filtered, washed with DI water again to remove H_2SO_4 residuals, and finally dried at 70 °C in an oven overnight under ambient air conditions. It is worth mentioning that organic DMF (dimethylformamide) solvent can replace concentrated H_2SO_4 in the above procedures to dissolve FePc or CoPc and lead to similar electrochemical measurement results for the prepared catalysts. In this work, we found that the carbon-supported FePc or CoPC catalysts prepared with the acid solvent have slightly better performance than those prepared with DMF solvent. Consequently, we here only present the results for the samples prepared with H_2SO_4.

The carbon-supported electrocatalyst Pt/Vulcan XC-72 (20 wt % metal on carbon) was purchased from BASF and used as received. Sodium hydroxide (J.T. Baker) was purchased with a certified ACS reagent grade and used as received. O_2 gas was purchased from Praxair. All aqueous suspensions used in this study were prepared with Millipore ultrapure water (18.2 MΩ·cm).

FePc/C or CoPc/C ink solutions were prepared by mixing 3 mg of the FePc/C or CoPc/C catalyst with 1 mL of ethanol, 1 mL of water, and 33 μL of 0.5% Nafion in an ultrasonic bath for 1 h. Comparative Pt/C (20% weight) ink was prepared by mixing 5 mg of Pt/C catalyst with 1.25 mL of ethanol, 1.25 mL of water, and 52.6 μL of 0.5% Nafion in an ultrasonic bath for 1 h.

II.2. Preparation of Electrodes. A grassy carbon (GC) disk electrode (Pine Instruments) with a 5.0 mm diameter was used as the working electrode. Before any measurements, the electrode surface was polished with an aqueous suspension of Al_2O_3 (0.05 μm) and rinsed with DI water. The GC electrode was then placed in an ultrasonic cleaning bath for 5 min and rinsed again with DI water. To absorb the molecule catalysts on it, the GC disk electrode was immersed into a dimethylformamide (DMF) solution containing 1.0×10^{-3} M FePc or CoPc and rotated at 500 rpm for 25 min. Then the electrode was rinsed with DI water and introduced into the electrochemical cell for the ORR stability test.

The working electrodes of FePc/C, CoPc/C, or Pt/C were made by dropping 40 μL of the corresponding ink solution on the surface of either the GC rotating disk electrode or the rotating ring-disk electrode. Then the deposited drop of ink was dried in an air-flow environment at room temperature to evaporate the solvent. Thus, an ultrathin film of FePc/C, CoPc/C, or Pt/C catalyst was formed on the GC surface. In this work, the three catalyst films have a nearly equal thickness, which is about 1.70 μm. On the basis of their densities, the metal loading on the disk electrode was estimated to be about 8.7 μg/cm^2 for Fe, 9.1 μg/cm^2 for Co, and 83 μg/cm^2 for Pt. It should be noted that the metal loadings are estimated here with the assumption that the catalyst molecules (FePc or CoPc) are completely dissolved in the concentrated H_2SO_4 acid solution and distributed uniformly in the ink when preparing the thin films. In this work, we did not conduct further measurements on the exact composition of the catalysts during the electrochemical tests.

II.3. Electrochemical Measurements. The electrochemical measurement setup consists of either a computer-controlled Solartron 1287 electrochemical interface or Pine bipotentiostat, a radiometer speed control unit from Pine Instrument Company (MSRX Speed Control), and a rotating ring-disk electrode radiometer (RRDE, glassy carbon with a diameter of 5.0 mm as the disk and Pt as the ring). The RDE and the RRDE experiments were conducted in an O_2-purged 0.1 M NaOH solution using a conventional standard three-electrode electrochemical cell with a jacket. A Pt wire counter electrode with a large surface area and a Hg/HgO reference electrode connected via a salt bridge were used. All the potentials in this work refer to Hg/HgO in a 0.1 M NaOH solution, denoted as Hg/HgO (about 0.164 V vs. NHE).

H_2O_2 production in O_2-saturated 0.1 M NaOH electrolytes was monitored in a RRDE configuration, using a polycrystalline Pt ring biased at 0.3 V vs. Hg/HgO. The ring current (I_r) was recorded simultaneously with the disk current (I_d). Collection efficiency (N) of the ring electrode was calibrated by $K_3Fe(CN)_6$ redox reaction in an Ar-saturated 0.1 M NaOH solution. The value of the collection efficiency ($N = I_r/I_d$) determined is 0.23 for both the FePc/C and the CoPc/C, and 0.26 for the Pt/C electrodes. The fractional yields of H_2O_2 in the ORR were calculated from the RRDE experiments as $X_{H_2O_2} = (2I_r/N)/(I_d + 2I_r/N)$. The mass transport normalized kinetic ORR currents at the disk electrode were calculated as $I_k = I_{lim}I/(I_{lim} - I)$, with limiting current (I_{lim}) taken as the ORR current at potential −0.4 or −0.5 or −0.6 V vs. Hg/HgO, respectively.

II.4. Computational Methods. DFT calculations were performed with the Materials Studio DMol3 module from Accelrys.[33] The generalized gradient approximation of Perdew and Wang[34] was used for exchange and correlation and the double numeric basis with polarization functions was used as the atomic basis set. Density functional semicore pseudopotentials, which were generated by fitting all electron relativistic DFT results, were used to reduce the computation cost. Spin-unrestricted wave functions and Fermi orbital occupations were used in our calculations. The energy convergence for geometry optimization was set to 1×10^{-5} eV.

III. Results

III.1. RDE and RRDE Measurements. Several important reaction parameters, such as the number of electrons involved in the ORR, Tafel slopes, and the kinetic rate constant for the ORR, can be obtained from RDE measurements. Figure 1 shows the rotating disk polarization curves at various rotation rates for oxygen reduction on a GC RDE electrode coated with the FePc/C (Figure 1a), the CoPc/C (Figure 1b), or the 20 wt % Pt/C (Figure 1c) catalyst in a 0.1 M NaOH solution saturated with oxygen. The onset ORR potential on the FePc/C electrode

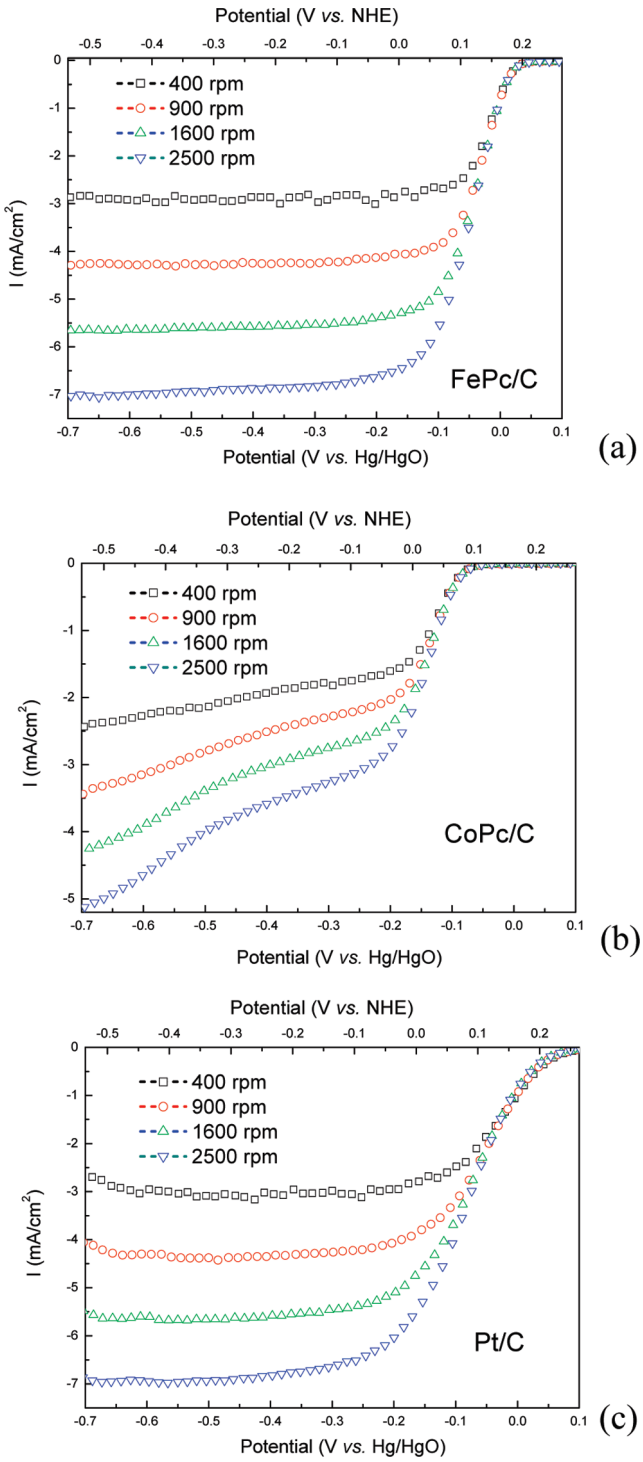

Figure 1. RDE polarization curves at different rotation rates for oxygen reduction on GC with predeposited (a) FePc/C, (b) CoPc/C, and (c) Pt/C in a 0.1 M NaOH solution saturated with oxygen. GC electrode area = 0.196 cm^2, scan rate = 10 mV s^{-1}, and room temperature. In the figure, the potentials are given with reference to both Hg/HgO electrode and normal hydrogen electrode (NHE). Note that the computed potential of the Hg/HgO electrode versus an NHE at 25 °C and 1 atm is 0.164 V for 0.1 M NaOH solution.

starts at the same potential (0.050 V vs. Hg/HgO) as that on the Pt/C electrode and shifts more than 100 mV positively as compared to that on the CoPc/C electrode. These results are in good agreement with previous ones reported in the literature.[35–39] For example, Behret et al.[35] reported the onset ORR potential to be 0.9 V vs. dynamic hydrogen electrode (DHE, −960 mV vs. Hg/HgO in 5 M KOH[36]) measured with a rotating FePc disk electrode in a 1 M KOH solution, and Tanaka et al.[37] showed the onset potential of O_2 reduction to be 0.050 V vs. Hg/HgO in a 1 M NaOH solution. Jiang et al.[38] reported that the onset potential for O_2 reduction on the Pt/C is around 0.050 V vs. Hg/HgO in a 0.1 M NaOH solution, corresponding to an overpotential of 0.190 V. M. Issacs et al.[39] showed the onset ORR potential on a CoPc electrode around −0.150 V vs. SCE in a 0.1 M NaOH solution.

Unlike in 0.1 M H_2SO_4 solution,[27] the polarization curves of the FePc/C electrode in 0.1 M NaOH solution (see, Figure 1a) display current plateaus in the high-polarization range. The mass transport limiting ORR current was reached at the potential less than −0.1 V vs. Hg/HgO on the FePc/C and less than −0.2 V vs. Hg/HgO observed on the CoPc/C. The mixed mass transport and kinetic controlled region was reached at the potentials from −0.1 to 0.05 V on the FePc/C, from −0.2 to −0.05 V on the CoPc/C, and from −0.2 to 0.05 V on the Pt/C. The half-wave potentials were around −0.050 V on the FePc/C, −0.100 V on the Pt/C, and −0.120 V on the CoPc/C. Our results here also agree well with what had been reported.[35,38,39] To examine the influence of Vulcan carbon on the catalytic performance of the catalysts, RDE experiments were also conducted on the electrodes with noncarbon-supported CoPc and FePc catalysts as well as with just Vulcan carbon. Comparing the curves for the same catalysts with and without carbon supports, we found that Vulcan-carbon contributes little toward the ORR current for the FePc/C catalysts but contributes appreciably to the ORR current for the CoPc/C catalysts.

The Koutecky−Levich equation[40] states that

$$I_{\lim} = 0.62nFD^{2/3}\nu^{-1/6}c_0\omega^{1/2} \quad (3)$$

where $I_{\lim}$ is the limiting current density, n is the number of electrons transferred per oxygen molecule, F is the Faraday constant (96500 C mol^{-1}), D is the O_2 diffusion coefficient (1.9 × 10^{-5} cm^2 s^{-1}) in 0.1 M NaOH, ν is the kinematic viscosity (1.1 × 10^{-2} cm^2 s^{-1}), C_O is the concentration of oxygen (1.2 × 10^{-6} mol cm^{-3}), and ω is the rotation rate in the radian.[16,39,41,42] Figure 2 shows the Koutecky−Levich plots of $1/I_{\lim}$ vs. $1/\omega^{1/2}$ at fixed potentials on the FePc/C (Figure 2a), the CoPc/C (Figure 2b), and the Pt/C (Figure 2c) electrodes derived from the data in Figure 1. From the slopes of the Koutecky−Levich plots, we calculated the electron exchange number (n) for ORR at the fixed potentials of −0.4, −0.5, and −0.6 V vs. Hg/HgO (mass transport regime). For both FePc/C and Pt/C, n is determined to be 3.8, agreeing well with what has been reported.[16,38] This result indicates that the O_2 reduction catalyzed on the FePc/C or on the Pt/C electrode is a $4e^-$ reduction process leading to OH as the main product. For the CoPc/C, n is in a range of 1.4 to 2.4, which is consistent with the data from another study.[39] This result suggests that the ORR catalyzed on the CoPc/C electrode is a $2e^-$ reduction process leading to H_2O_2.

To further verify the ORR pathways on the FePc/C and the CoPc/C electrodes, we carried out RRDE measurements to monitor the formation of H_2O_2 during the ORR process. Figure 3 gives the RRDE polarization curves for O_2 reduction on the FePc/C, CoPc/C, and Pt/C with a rotation rate of 2500 rpm in 0.1 M NaOH solution saturated with oxygen. The inset of Figure 3 gives the H_2O_2 yields on the three catalysts. On both FePc/C and Pt/C electrodes, no significant solution phase H_2O_2 was detected and thus the H_2O_2 yield was negligible. For the CoPc/C electrode, a significant ring current was detected starting at the ORR onset potential of the disk electrode and up to 50% of the

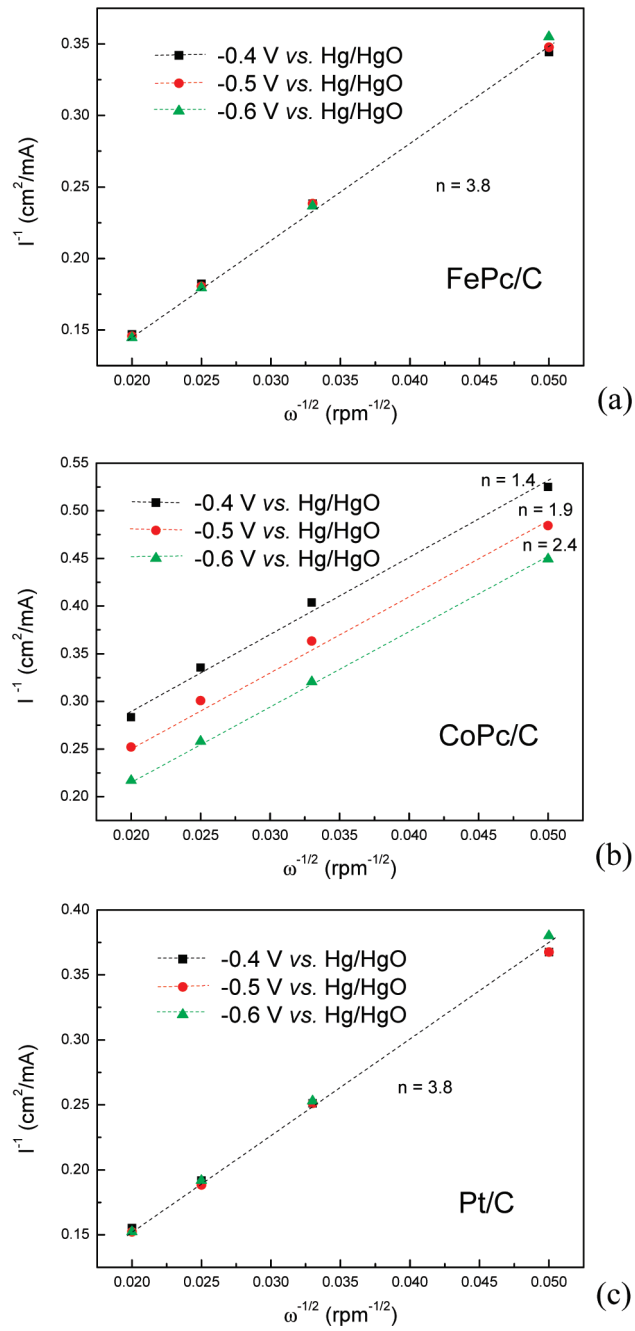

Figure 2. Plot of I^{-1} vs. $\omega^{-1/2}$ for oxygen reduction on GC with precoated (a) FePc/C, (b) CoPc/C, and (c) Pt/C catalysts in a 0.1 M NaOH solution saturated with oxygen at potentials −0.4, −0.5, and −0.6 V vs. Hg/HgO.

H_2O_2 yield was measured. This result indicates that H_2O_2 is a main product for the ORR catalyzed by the CoPc/C but not for ORR catalyzed by the FePc/C. Referencing eqs 1 and 2, the RRDE results confirm our results calculated from the Levich equation that the ORR electron exchange number is 3.8 (close to $4e^-$) for the ORR on the FePc/C and Pt/C, but about 2 ($2e^-$) for the ORR on the CoPc/C.

Figure 4 presents the mass-corrected Tafel plots of log I_k (mA cm^{-2}) vs. the electrode potential E for the ORR on the FePc/C, the CoPc/C, and the Pt/C electrodes in an O_2-saturated 0.1 M NaOH solution. These Tafel curves were derived from the polarization curves of Figure 1 with a rotation rate of 2500 rpm. The Tafel slopes (listed in Table 1) for the FePc/C and Pt/C catalysts are quite similar and can be divided into two parts, i.e., about 50 mV dec^{-1} at the lower overpotential region (where $E > 0$ V vs. Hg/HgO) and about 120 mV dec^{-1} at the higher overpotential region (where $E < -100$ mV vs. Hg/HgO). These results correspond well with those reported in the literature[16,38] and imply that the rate-determining step of the ORR is similar for both the FePc/C and Pt/C catalysts. The Tafel slope of the CoPc/C catalyst is around 120 mV dec^{-1} at the higher overpotential region (where $E < -150$ mV vs. Hg/HgO), corresponding well with what were reported by M. Issacs et al.[39] At a typical alkaline fuel cell cathode working potential (−0.05 V vs Hg/HgO, equivalent to an overpotential of 0.280 V), the ORR kinetic current on the FePc/C is 10 mA cm^{-2}, which is about 3 times higher than that of the Pt/C electrode (3.1 mA cm^{-2}). In a pure oxygen and 0.1 M NaOH electrolyte environment, the FePc/C displays better performance than both the 20 wt % Pt/C and the CoPc/C.

A rapid decline of the catalytic activity for ORR on both unsupported and carbon-supported M-N_4-macrocycles electrocatalysts has been reported.[25,27,43–45] To examine the stability of FePc and CoPc as electrocatalysts for ORR, we performed potentiostatic measurements with a potential set at −0.100 V vs. Hg/HgO on the FePc/C and the CoPc/C electrodes with a rotating rate of 900 rpm in O_2-saturated 0.1 M NaOH solutions. The ORR current density at the held potential was recorded for 6000 s and shown in Figure 5a. The ORR current density on the FePc/C electrode was found to be more than an order of magnitude higher than that on the CoPc/C, but declined quickly with test time at a rate of 0.1 μA cm^{-2} s^{-1}. In contrast, the ORR current density on the CoPc/C electrode remains constant. It infers that the FePc/C does not have as good stability as the CoPc/C catalyst for ORR in alkaline solutions. However, the comparison in Figure 5a between the FePc/C and CoPc/C in their stability is not convincingly conclusive because the carbon-supported FePc and CoPc may degrade differently under different operation currents and cause the observed discrepancy. To address that problem, we further performed RDE cycling tests on the FePc and CoPc catalysts without carbon supports adsorbed to a GC electrode with a scanning rate at 10 mV/s and a rotating rate of 2500 rpm in oxygen-saturated 0.1 M NaOH solutions. As shown in Figure 5b, the FePc catalyst without carbon supports also displayed a significant reduction in its ORR current density with each continuing cycle, while the CoPc catalyst showed less obvious ORR current density reductions. Hence, our results show clearly that the FePc with or without carbon supports has less ORR electrocatalytic stability than the CoPc under fuel cell operation conditions.

A performance recovery experiment was conducted on the FePc catalyst preadsorbed on a GC RDE surface. Figure 6 displays the results from this experiment. We first run a cyclic voltammogram test on the RDE electrode preadsorbed FePc molecules for 30 cycles by sweeping potentials from −0.700 to 0.100 V vs. Hg/HgO in an oxygen-saturated 0.1 M NaOH solution with scanning rate at 10 mV s^{-1}. As shown in Figure 6, the catalytic activity of the FePc catalyst dropped dramatically at the end of the 30th cycle. Then, we left the electrode in the same alkaline solution for 12 h. Further, a new electrochemical measurement on the same electrode was performed in the 0.1 M NaOH solution saturated with oxygen. A noticeable recovery in the catalytic activity of the FePc catalyst for ORR could be clearly observed in Figure 6. However, the catalytic performance of the FePc could not be fully recovered.

III.2. DFT Calculations. According to eqs 1 and 2, we know that O_2 and H_2O molecules are reactants, OH molecule is a product via both the $4e^-$ and the $2e^-$ paths, while HOOH

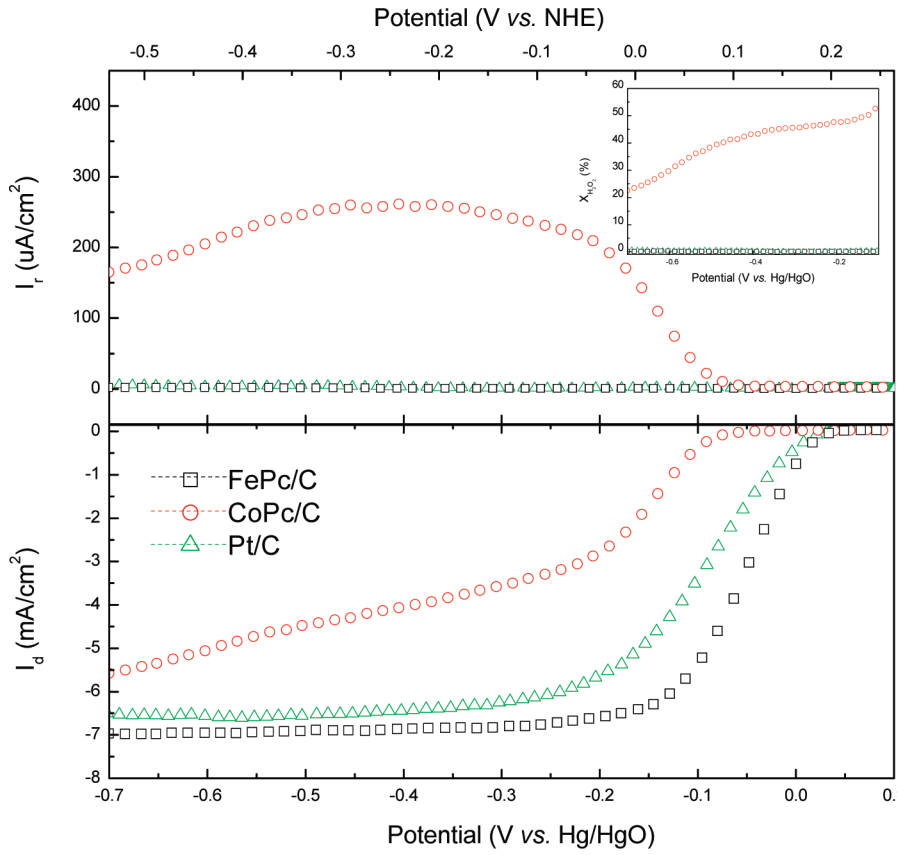

Figure 3. RRDE measurements of the ORR on the FePc/C, CoPc/C, and Pt/C electrodes with a rotation rate of 2500 rpm in a 0.1 M NaOH solution during positive scanning. Scan rate = 10 mV s^{-1}. In the figure, the potentials are given with reference to both Hg/HgO electrode and normal hydrogen electrode (NHE). Note that the computed potential of the Hg/HgO electrode versus an NHE at 25 °C and 1 atm is 0.164 V for 0.1 M NaOH solution.

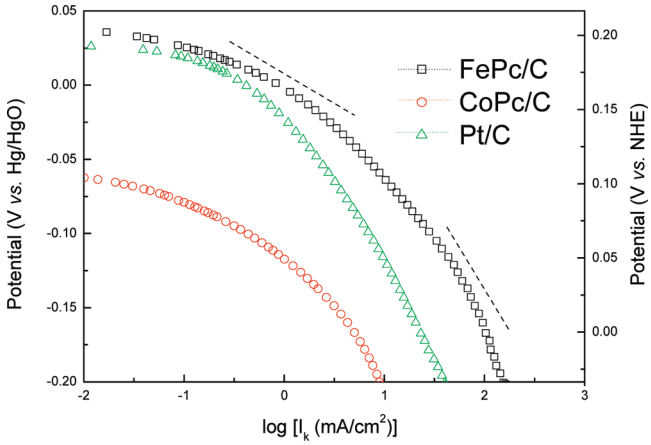

Figure 4. Tafel plots of log I_k vs. E (V) for the ORR on the FePc/C, CoPc/C, and Pt/C electrodes in an oxygen-saturated 0.1 M NaOH solution at a rotation rate of 2500 rpm. Limiting current density obtained at potential −0.5 V vs. Hg/HgO was used to calculate I_k. GC electrode area = 0.196 cm^2, room temperature. In the figure, the potentials are given with reference to both Hg/HgO electrode and normal hydrogen electrode (NHE). Note that the computed potential of the Hg/HgO electrode versus an NHE at 25 °C and 1 atm is 0.164 V for 0.1 M NaOH solution.

(hydrogen peroxide) and H_2OO (oxywater) are the two isomers of H_2O_2, which is another product molecule via the two-electron route. To elucidate the reaction pathway of the ORR on FePc and CoPc catalyst molecules, we performed DFT calculations to determine the structure and energy of O_2, H_2O, OH, HOOH, and H_2OO molecule adsorption on the surfaces of the FePc and the CoPc molecules.

TABLE 1: Tafel Slopes (mV dec^{-1}) for FePc/C, CoPc/C, and Pt/C at Different Voltages

catalysts	low η (at $E > 0$ V)	high η ($E < -0.100$ V)
FePc/C	42	120
CoPc/C		127
Pt/C	47	128

The optimized structure for the above adsorption systems was obtained through structural optimization calculations using the DFT method implemented in Dmol3. After attaining the optimized structures, we calculated the adsorption energy for those molecules on the phthalocyanine molecules. The adsorption energy is defined as the energy difference between the adsorption and the isolated systems. Here, the energy of the isolated system refers to the sum of the energies of the relaxed phthalocyanine and the individual adsorbate molecules. Therefore, negative adsorption energy indicates that the adsorbate molecule would be energetically favorable to be adducted to the surface of the FePc and the CoPc catalysts, while positive adsorption energy means that the adsorbate molecule would not be energetically favorable to make contact with the FePc and the CoPc catalysts. Consequently, the negative adsorption energy of the O_2 molecule on the surface of the catalysts is a requirement for the catalysts to promote ORR.

In Table 2, we give the predicted adsorption energy for the most stable (namely, the lowest energy) adsorption configuration of those molecules on FePc and CoPc. Moreover, we plotted in Figure 7 the optimized lowest energy molecular structures of O_2, H_2O, and OH adsorbed on FePc or CoPc. It can be noted that O_2, H_2O, and OH molecules assume the same configuration as their most stable adsorption on both FePc and CoPc

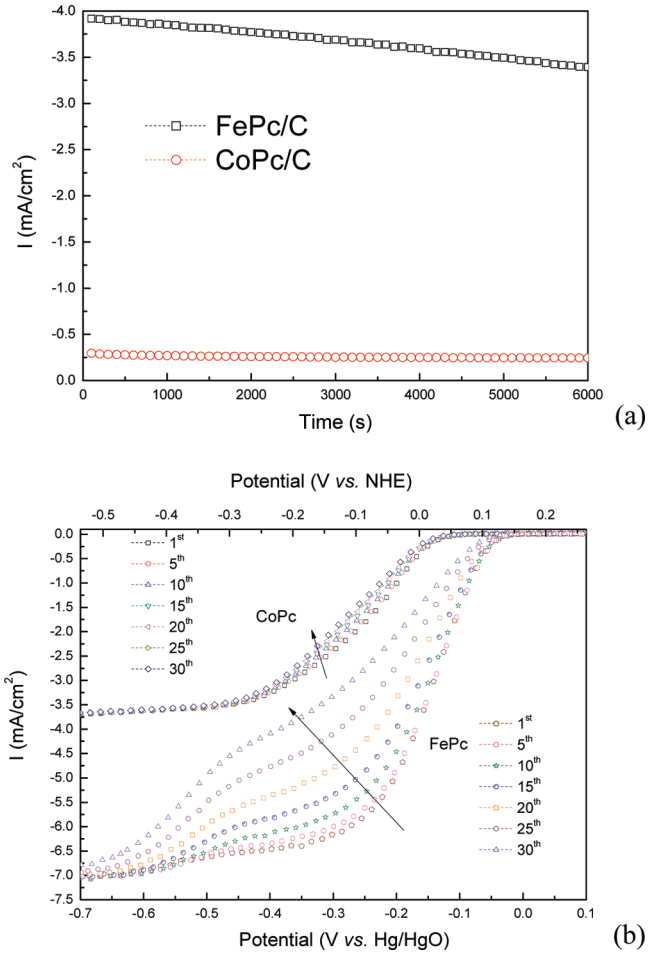

Figure 5. The stability test for FePc and CoPc precoated on a GC electrode at a rotating rate of 900 rpm in oxygen-saturated 0.1 M NaOH at room temperature. (a) Potentiostatic measurements at −0.1 V vs. Hg/HgO on FePc/C and CoPc/C at 900 rpm; (b) cycling test on FePc and CoPc preadsorbed on a GC electrode with a scanning rate 10 mV s^{-1} at a rotating rate of 2500 rpm. In the figure, the potentials are given with reference to both Hg/HgO electrode and normal hydrogen electrode (NHE). Note that the computed potential of the Hg/HgO electrode versus an NHE at 25 °C and 1 atm is 0.164 V for 0.1 M NaOH solution.

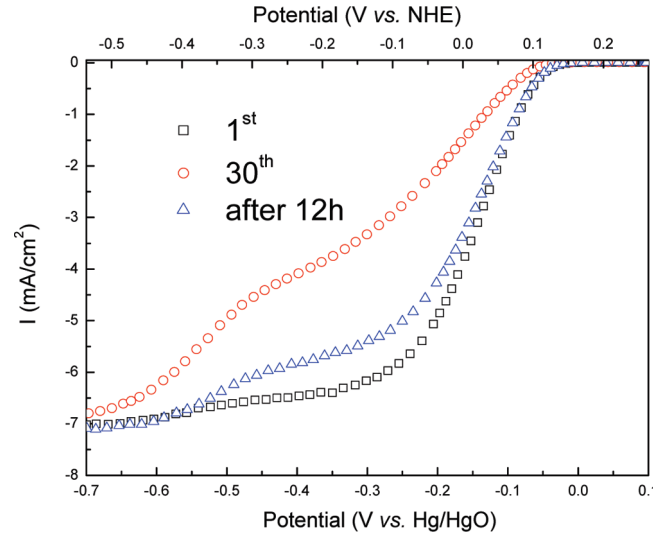

Figure 6. The performance recovery test for FePc preadsorbed on a GC rotating disk electrode surface at a rotating rate of 2500 rpm in oxygen-saturated 0.1 M NaOH at room temperature with a scanning rate 10 mV s^{-1}. In the figure, the potentials are given with reference to both Hg/HgO electrode and normal hydrogen electrode (NHE). Note that the computed potential of the Hg/HgO electrode versus an NHE at 25 °C and 1 atm is 0.164 V for 0.1 M NaOH solution.

TABLE 2: Calculated Adsorption Energy (in units of eV) of Reactant (O_2 and H_2O), Product (OH), and Reaction Intermediate (HOOH and H_2OO) Molecules Adsorbed on FePc and CoPc Catalyst Molecules Using the First-Principle DFT Method[a]

	O_2	H_2O	OH	HOOH	H_2OO
FePc	−1.16	−1.05	−3.41	−1.05	−1.03
CoPc	−0.40	−0.32	−2.36	−0.24	−0.47
Pt (111)	−0.79	−0.20	−2.39		

[a] For comparison, the adsorption energy of O_2, H_2O, and OH molecules on a Pt (111) surface is also listed. These adsorption energies on the Pt (111) surface were calculated with VASP software and the plane wave pseudopotential method.

molecules. In the most stable adsorption of O_2, one O atom lies right above the central metal atom over the catalyst molecule plane, the other O atom is farther away from the metal atom, and the projection of the O−O bond axis on the catalyst molecule plane is aligned with the bisecting line of the two neighboring bonds between the central metal atom and the two nearest N atoms. In the most stable adsorption of H_2O, the O atom lies right above the central metal atom over the catalyst molecule plane, the H_2O molecule is nearly parallel to the catalyst molecule plane, and the projection of the H−O−H bond angle on the catalyst molecule plane is bisected by the connecting line between the central metal atom and one of its nearest N atoms. In the most stable adsorption of OH, the O atom lies right above the central metal atom over the catalyst molecule plane, the H atom is extended away from the metal atom, and the projection of the O−H bond axis on the catalyst molecule plane is aligned with the bond between the central metal atom and one of its nearest N atoms.

Furthermore, we optimized all the possible structures of HOOH and H_2OO molecules adsorbed on the catalyst molecules (shown in Figure 8). We determined the adsorption energy for HOOH on FePc to be −0.99 (Figure 8a), −1.01 (Figure 8b), −1.05 (Figure 8c), and −0.32 eV (Figure 8d). We found the adsorption energy for H_2OO on FePc to be −0.94 (Figure 8e) and −1.03 eV (Figure 8f). Thus, the configuration shown in Figure 8c is the lowest energy structure for H_2O_2 adsorbed on the FePc molecule. For HOOH on CoPc, we found that parts a and b of Figure 8 are energy favorable configurations, but parts c and d of Figure 8 are not. The adsorption energy for HOOH on CoPc was predicted to be −0.24 (Figure 8a) and −0.22 eV (Figure 8b). We calculated the adsorption energies of H_2OO on CoPc to be −0.47 (Figure 8e) and −0.45 eV (Figure 8f). Consequently, the configuration shown in Figure 8e turns out to be the lowest energy structure for H_2O_2 adsorbed on the CoPc molecule.

IV. Discussion

Our theoretical calculation results reveal molecular details about the ORR mechanisms on FePc and CoPc catalyst molecules, which enables us to better interpret our experimental observations, such as the ORR onset potentials, reaction pathways ($4e^-$ or $2e^-$), and stability of these catalysts.

IV.1. Oxygen Adsorption To Be the Key Step To Control the ORR Onset Potential. First, we compare the adsorption energy of the two reactant (O_2 and H_2O) molecules on the surface of the three catalysts (FePc, CoPc, and Pt (111)). Our

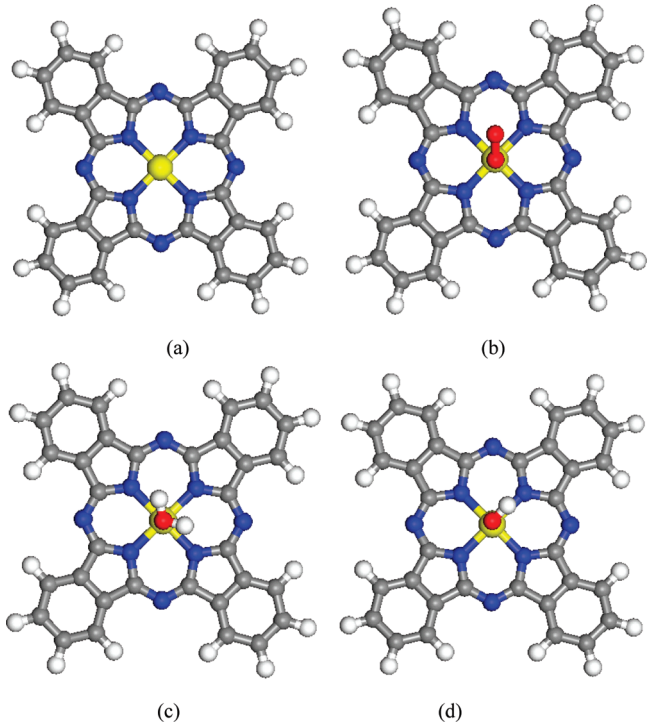

Figure 7. Optimized lowest energy structure of (a) isolated FePc or CoPc catalyst molecules, (b) O_2 adsorbed on FePc or CoPc, (c) H_2O adsorbed on FePc or CoPc, and (d) OH adsorbed on FePc or CoPc. The central yellow ball represents a metal Fe or Co atom, blue balls represent N atoms, gray balls represent C atoms, and light white balls represent H atoms.

results in Table 2 point out that the O_2 molecule would have a lower adsorption energy, and hence, it would bind more strongly to the three catalysts than the H_2O molecule. Since FePc and CoPc molecules only provide one adsorption site (the central metal atom), this result suggests that the adsorption of the O_2 (not the H_2O) molecule on FePc and CoPc would be the first step of the ORR in an alkaline solution. Moreover, our results in Table 2 show that the adsorption energies of O_2 on the catalysts follow the increasing order of FePc, Pt (111), and CoPc, which correlates well with our experimental observations (shown in Figures 1 and 3). FePc/C catalyst shows the most positive ORR onset potential, which is more than the Pt/C catalyst and much more than the CoPc/C catalyst. On the basis of the slopes of the Tafel plots (Figure 4), the rate-determining step for ORR was considered to be similar on both the FePc/C and the Pt/C electrodes. It is well believed that O_2 adsorption is a limiting step for the ORR on Pt surface. Therefore, we conclude that the O_2 adsorption process is a limiting step affecting the kinetics of the ORR on FePc and CoPc: the lower the O_2 adsorption energy, the higher the kinetics of the ORR on the molecular catalysts. Yeager et al.[37] had postulated earlier that the affinity of Fe(II)Pc for O_2 may be very high compared to that for the reaction intermediates, products, or other solution-phase components and suggested that this strong interaction with O_2 compared to that with other species can be of critical importance to the electrocatalytic activity involving a single type of iron site. Consequently, our finding in this work supports such a proposition that O_2 adsorption plays a key role in the activation and reduction of oxygen.

IV.2. H_2O_2 Adsorption To Distinguish the $4e^-$ or $2e^-$ Routes of the ORR on FePc vs. CoPc. The ORR would assume the $4e^-$ route on FePc molecule catalysts but take the $2e^-$ routes on CoPc molecule catalysts. As shown in Figure 3, we

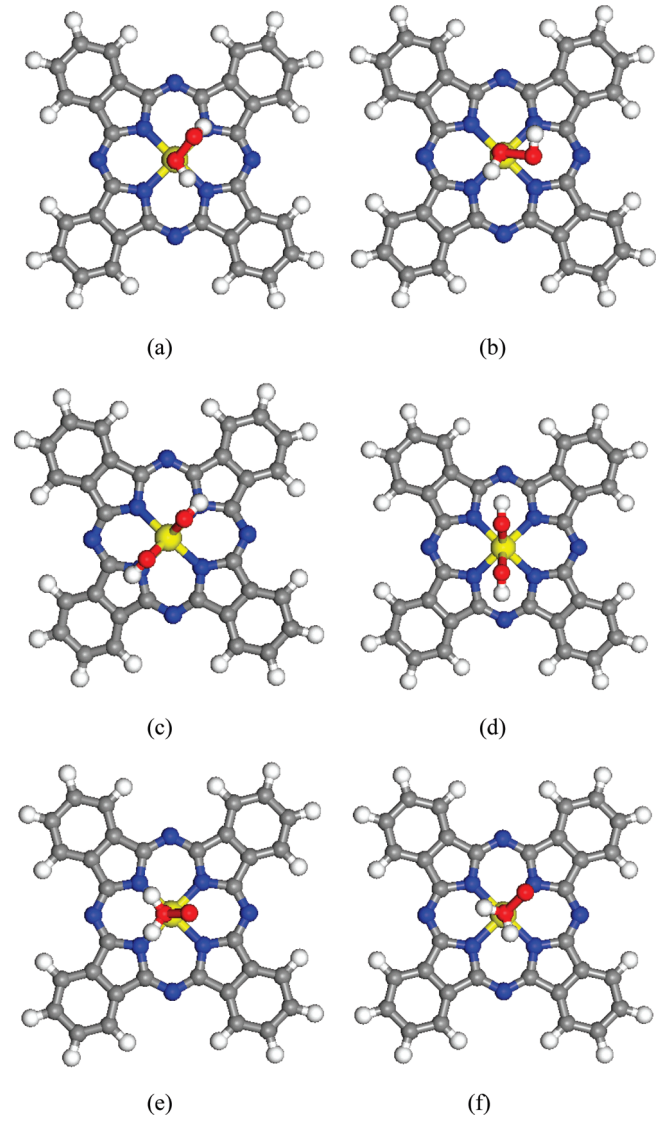

Figure 8. Optimized structural configurations for HOOH (a−d) and H_2OO (e and f) molecules adsorbed on FePc/CoPc molecules. The central yellow ball represents the metal Fe/Co atom, the two red balls represent O atoms, blue balls represent N atoms, gray balls represent C atoms, and light white balls represent H atoms.

demonstrated that no H_2O_2 was detected on the FePc/C electrodes, but significant amounts of H_2O_2 were observed on the CoPc/C electrodes with the starting potential the same as the ORR onset potential of the disk electrode. Our theoretical calculations provide an explanation as to why this happens.

On FePc molecules at the lowest energy state, H_2O_2 will have a geometric structure as shown in Figure 8c. DFT calculation predicts in Figure 8c that the two O atoms in an H_2O_2 molecule bind to the common central Fe atom with a distance of 1.820 Å, bind to individual H atoms with a distance of 0.972 Å, but are separated from each other by a distance of 2.368 Å. In an isolated HOOH molecule, the O−O bond length is calculated to be 1.487 Å. Hence, O−O bond breaking, which is a prerequisite for four-electron ORRs, will occur during the process of H_2O_2 adsorption on FePc molecules. In contrast, Figure 8c shows an unfavorite adsorption configuration for HOOH on CoPc molecules. Instead, the H_2O_2 molecule prefers to have the configuration of Figure 8e when adsorbed on CoPc. In that optimized configuration, the two O atoms in the H_2O_2 molecule are only distanced by 1.536 Å, which is very close to the equilibrium O−O bond length of 1.501 Å in an isolated

H_2OO molecule. Clearly, O−O bond breaking does not happen during the process of H_2O_2 adsorption on CoPc molecules. Therefore, our DFT calculations about the H_2O_2 adsorption process strongly indicate that the breaking of the O−O bond accounts for the $4e^-$ ORR on the FePc catalyst molecule, while the lack of the O−O bond breaking leads to the $2e^-$ ORR on the CoPc catalyst molecule.

IV.3. OH Adsorption To Be a Key Factor for Cycling Stability of FePc and CoPc. Compared to O_2, OH will have even lower adsorption energy and hence a more energetically favorable adsorption on FePc and CoPc molecules based on our DFT calculation results given in Table 2. Since radical OH is a product of the ORR regardless of the reaction paths ($4e^-$ or $2e^-$), the generated OH might occupy those active reaction sites on the surface of the catalysts after the ORR and prevent further adsorption of O_2. Conceivably, this will cause a degradation of the performance of the molecule catalysts. Using the data in Table 2, we derived that the difference in the adsorption energy of O_2 and OH is about 2.25 eV on FePc and 1.96 eV on CoPc. Thus, this implies that the performance degradation caused by OH would be more severe for FePc than it would be for CoPc molecule catalysts. In Figure 5, we showed that ORR activity of FePc declined much more rapidly than that on CoPc with either continually cycling or holding at a constant potential. Thus, experimental observation on the stability of catalysts is consistent with what was predicted by the DFT calculations based on OH adsorption. Furthermore, we showed in Figure 6 that the catalytic activity of the FePc/C can be partially recovered simply by leaving the catalysts in a 0.1 M NaOH solution for some time. It is reasonable to interpret the partial recovery of the catalytic activity as a result of the removal of the adsorbed OH on FePc catalysts owing to OH diffusion processes in alkaline solution. After the adsorbed OH is diffused away from the FePc molecules, the catalysts regain their active sites for oxygen molecule adsorption. Thus, the results in Figure 6 would further support our proposal that the strong OH adsorption on the FePc molecule is responsible for the performance degradation of the FePc catalyst. Moreover, the fact that the catalytic performance could not be fully recovered implies that some irreversible processes, like molecule decomposing and/or central transition metal atom removal, would also occur during the cycle tests.

V. Conclusions

Using RDE and RRDE techniques and DFT calculations, we elucidated the mechanisms of the ORR on carbon-supported FePc and CoPc catalysts. In our electrochemical measurements, FePc/C displays not only more than 100 mV positive ORR onset potential and half-wave potential, but also more than double the limiting current than CoPc/C. Our DFT calculations gave O_2 adsorption energy of −1.16 eV on FePc and −0.40 eV on CoPc molecules. Correlating the experiment with theory, we infer that oxygen adsorption on the catalysts is the key step to control the ORR onset potential. For the molecular catalysts, the lower the O_2 adsorption energy, the higher the kinetics of the ORR that can be expected. Moreover, our electrochemical measurements show that FePc/C catalysts were found to promote the desired $4e^-$ ORR in alkaline solutions while CoPc/C only facilitates $2e^-$ ORR. Corresponding to that observation, our DFT calculations indicate that the ORR pathways, $2e^-$ or $4e^-$, are mostly determined by the structures of H_2O_2 adsorption on FePc and CoPc catalysts. The breaking of the O−O bond during H_2O_2 adsorption accounts for the $4e^-$ ORR on FePc catalyst molecule, while the lack of the O−O bond breaking process leads to the $2e^-$ ORR on CoPc catalyst molecule. Third, we believe that OH adsorption on the catalysts is an important factor to determine the stability of the FePc and CoPc catalysts. It was predicted from DFT calculations that OH adsorption is more energetically favorable than O_2 adsorption on both FePc and CoPc catalyst molecules. This will cause the produced OH molecule to occupy the active sites of catalysts and hamper further progress (O_2 adsorption) of ORR. Our DFT result implies that this degradation process should be more severe for FePc than CoPc, due to a larger energy gain when adsorbing OH instead of O_2 on the FePc surface. Concurring with DFT work, our experimental stability tests showed clearly that the FePc/C catalyst will lose its performance much more quickly than the CoPc/C catalyst.

Thus, we have demonstrated that the combination of electrochemical measurements (RDE and RRDE) and theoretical modeling is a powerful approach in identifying high-performance catalysts for ORR and investigating the ORR mechanisms. Our study suggests that the FePc/C is a promising nonprecious electrocatalyst and can be applied in alkaline fuel cells. The ORR on FePc/C catalyst has a quite positive onset potential and half-wave potential, and adopts a high energy capacity $4e^-$ reaction path. However, the FePc/C catalyst will lose its catalytic activity rapidly under fuel cell working conditions. Understanding the mechanisms underlying those observations as presented in this paper is essential for us to further tailor the chemistry of the catalyst molecules for the purpose of finding an economic, active, and durable catalyst for SAFCs.

Acknowledgment. This work was supported by the U.S. Army Research Lab (Grant No: W911NF-07-2-0036).

References and Notes

(1) Varcoe, J. R. *RCT Slade, Fuel Cells* **2005**, *5*, 187.
(2) Spendelow, J. S.; Wieckowski, A. *Phys. Chem. Chem. Phys.* **2007**, *9*, 2654.
(3) Varcoe, J.; Slade, R.; Wright, G.; Chen, Y. *J. Phys. Chem. B* **2006**, *110*, 21041.
(4) Varcoe, J.; Slade, R.; Yee, E. *Chem. Commun.* **2006**, 1428.
(5) Park, J.; Park, S.; Yim, S.; Yoon, Y.; Lee, W.; Kim, C. *J. Power Sources* **2008**, *178*, 620.
(6) Matsuoka, K.; Iriyama, Y.; Abe, T.; Matsuoka, M.; Ogumi, Z. *J. Power Sources* **2005**, *150*, 27.
(7) Coutanceau, C.; Demarconnay, L.; Lamy, C.; Leger, J.-M. *J. Power Sources* **2006**, *156*, 14.
(8) Unlu, M.; Zhou, J.; Kohl, P. *Electrochem. Solid-State Lett.* **2009**, *12*, B 27.
(9) Fujiwara, N.; Siroma, Z.; Yamazaki, S.; Ioroi, T.; Senoh, H.; Yasuda, K. *J. Power Sources* **2008**, *185*, 621.
(10) Zhou, J.; Unlu, M.; Vega, J.; Kohl, P. *J. Power Sources* **2009**, *190*, 285.
(11) Wang, G.; Weng, Y.; Chu, D.; Xie, D.; Chen, R. *J. Membr. Sci.* **2009**, *326*, 4.
(12) Wang, G.; Weng, Y.; Zhao, J.; Chu, D.; Xie, D.; Chen, R., *Polym. Adv. Technol.* In press.
(13) Jiang, L.; Hsu, A.; Chu, D.; Chen, R. *J. Electrochem. Soc.* **2009**, *156*, B370.
(14) Jiang, L.; Hsu, A.; Chu, D.; Chen, R. *J. Electrochem. Soc.* **2009**, *156*, B643.
(15) Zagal, J.; Sen, R.; Yeager, E. *J. Electroanal. Chem.* **1977**, *83*, 207.
(16) Zagal, J.; Bindra, P.; Yeager, E. *J. Electrochem. Soc.* **1980**, *127*, 1506.
(17) Yeager, E. *Electrochim. Acta* **1984**, *29*, 1527.
(18) Van Der Putten, A.; Elzing, A.; Visscher, W.; Barendrecht, E. *J. Electroanal. Chem.* **1986**, *214*, 523.
(19) Collman, J.; Marrocco, M.; Danisovich, P.; Koval, C.; Anson, F. *J. Electroanal. Chem.* **1979**, *101*, 117.
(20) Collman, J.; Danisovich, P.; Konai, Y.; Marrocco, M.; Koval, C.; Anson, F. *J. Am. Chem. Soc.* **1980**, *102*, 6027.
(21) Liu, H.; Weaver, M.; Wang, C.; Chang, C. *J. Electroanal. Chem.* **1983**, *145*, 439.
(22) Yeager, E. *J. Mol. Catal.* **1986**, *38*, 5.

(23) Tse, Y.; Janda, P.; Lam, H.; Zhang, J.; Pietro, W.; Lever, A. B. P. *J. Porphyrins Phthalocyanines* **1997**, *1*, 3.
(24) Ramirez, G.; Trollund, E.; Isaacs, M.; Armijo, F.; Zagal, J.; Costamagna, J.; Aguirre, M. J. *Electroanalysis* **2002**, *14*, 540.
(25) Jagal, J. H., *N4-Macrocyclic Metal Complexes*, 1st ed.; Springer: New York, 2006.
(26) Barnanton, S.; Couranceau, C.; Roux, C.; Hahn, F.; Leger, J.-M. *J. Electroanal. Chem.* **2005**, *577*, 223.
(27) Baker, R.; Wilkinson, D.; Zhang, J. *Electrochim. Acta* **2008**, *53*, 6906.
(28) Schulenburg, H.; Stankov, S.; Schnemann, V.; Radnik, J.; Dorbandt, I.; Fiechter, S.; Bogdanoff, P.; Tributsch, H. *J. Phys. Chem. B* **2003**, *107*, 9034.
(29) Nørskov, J. K.; Rossmeisl, J.; Logadottir, A.; Lindqvist, L.; Kitchin, J. R.; Bligaard, T.; Jónsson, H. *J. Phys. Chem. B 108* **2004**, 17886.
(30) Nilekar, A. U.; Mavrikakis, M. *Surf. Sci.* **2008**, *602*, L89.
(31) Roques, J.; Anderson, A. B. *J. Electrochem. Soc.* **2004**, *151*, E340.
(32) Wang, G.; Ramesh, N.; Hsu, A.; Chu, D.; Chen, R. *Mol. Simul.* **2008**, *34*, 1051.
(33) *Materials Studio 4.1, Dmol3*; Accelrys Inc.: San Diego, CA.
(34) Perdew, J. P. Wang, Y. *Phys. Rev. B* **1992**, *45*, 13244.
(35) Behret, H.; Binder, H.; Sandstede, G.; Scherer, G. G. *J. Electroanal. Chem.* **1981**, *117*, 29.
(36) Goldstein, R.; Tesung, A. C. C. *J. Phys. Chem.* **1972**, *76*, 3646.
(37) Tanaka, A. A.; Fierro, C.; Scherson, D.; Yeager, E. B. *J. Phys. Chem.* **1987**, *91*, 3799.
(38) Jiang, L.; Hsu, A.; Chu, D.; Chen, R. *J. Electroanal. Chem.* **2009**, *629*, 87.
(39) Issacs, M.; Aguirre, M. J.; Toro-Labbe, A.; Costamagna, J.; Paez, M.; Zagal, J. H. *Electrochim. Acta*, **1998**,*43*, 1821.
(40) Bard, A. J.; Faulken, L. R. *Electrochemical Methods: Fandamental and Applications*, 2nd ed.; Wiley: New York, 2001.
(41) Tanaka, A.; Fierro, C.; Scherson, D.; Yeager, E. *Mater. Chem. Phys.* **1989**, *22*, 431.
(42) Morcos, I.; Yeager, E. *Electrochim. Acta* **1970**, *15*, 953.
(43) Zhang, J.; Tse, Y.; Pietro, W.; Lever, A. B. P. *J. Electroanal. Chem.* **1996**, *406*, 203.
(44) Kobayashi, N.; Janda, P.; Lever, A. B. P. *Inorg. Chem.* **1992**, *31*, 5172.
(45) Zecevic, S.; Simi-Glavaski, B.; Yeager, E.; Lever, A. B. P.; Minor, P. C. *J. Electroanal. Chem.* **1985**, *196*, 339.

JP906408Y